Tailoring the Thermotropic Behavior of Tetra-Substituted Phthalocyanines via the Lateral Chains Architecture

Raluca I. Gearba,[†] Alexander I. Bondar,[†] Bart Goderis,[‡] Wim Bras,[§] and Dimitri A. Ivanov*[,†]

Laboratoire de Physique des Polymères, CP-223, Université Libre de Bruxelles, Bld. du Triomphe, B-1050, Brussels, Belgium, Chemistry Department, Catholic University of Leuven, Celestijnenlaan 200F, 3001 Heverlee-Leuven, Belgium, and Netherlands Organization for Scientific Research (NWO), DUBBLE-CRG/ESRF, B.P. 220, F-38043 Grenoble Cedex, France

Received January 24, 2005. Revised Manuscript Received April 1, 2005

Four newly synthesized alkoxy tetrasubstituted phthalocyanines (Pcs) were characterized by polarized optical microscopy, differential scanning calorimetry, and X-ray diffraction on oriented samples. It was found that the introduction of lateral alkyl chains branched in the second position renders the material liquid crystalline at room temperature. The studied Pcs exhibit a transition between a columnar hexagonal and a columnar rectangular phase. The tilt of the molecules with respect to the columnar axis in the rectangular phase, as measured by X-ray fiber diffraction, was found to be 15−18°. The columnar structure, and defects therein, in relatively thick spin-coated mesomorphic Pc films were for the first time characterized by tapping mode atomic force microscopy, employing ultra-sharp tips with nanometer-thick whiskers. Spin-coated films reveal layerlike structure with domain boundaries that can induce significant columnar curvature without breaking of the columns. In some instances, the boundaries delimiting different LC domains completely disrupt the columnar structure making the columns in neighboring regions uncorrelated.

Introduction

Since the very discovery of mesogenic phthalocyanines (Pcs) by Piechocki and coauthors in 1982,[1] there has been a great, and growing, interest in these materials due to their fascinating optical and electronic properties,[2−5] which make them potential candidates for optoelectronic devices. Numerous derivatives of the Pc family have been created by varying the number, type, length, and position of the flexible substituents, as well as by incorporation of a metal ion in the cavity of the Pc molecule.[6−12] It should be noted that so far only a few members of the Pc family were found to exhibit liquid crystalline behavior at room temperature (RT).[13,14] Pcs can show self-assembly via cofacial stacking of molecular cores in both crystalline and liquid crystalline phases. The latter are more suitable for applications in electronic devices due to their improved processing characteristics such as self-healing of structural defects. The work by Collard et al.[15] demonstrated that the introduction of branched side-chains decreases both the clearing and the crystal-to-mesophase transition temperatures of discotic liquid crystals. Complete suppression of crystallization for Pcs has been achieved for the first time by Schouten et al.[13] who followed the same strategy. Recently it was found that charge carrier mobility is not significantly affected by the substitution of linear chains by branched ones, which can in some instances result in a tilt of molecules in the column.[16,17] This finding increases the value of the mentioned synthesis strategy for the design of novel technological Pc derivatives.

* To whom correspondence should be addressed. E-mail: divanov@ulb.ac.be.
† Université Libre de Bruxelles.
‡ University of Leuven.
§ Netherlands Organization for Scientific Research.

(1) Piechocki, C.; Simon, J.; Skoulios, A.; Guillon, D.; Weber, P. *J. Am. Chem. Soc.* **1982**, *104*, 5245−5247.
(2) Simon, J.; Bassoul, P. *Phthalocyanines Properties and Applications*; VCH: New York, 1993; Chapter 6.
(3) Schouten, P. G.; Warman, J. M.; de Haas, M. P.; Fox, M. A.; Pan, H. L. *Nature* **1991**, *353*, 736−737.
(4) Warman, J. M.; de Haas, M. P.; van der Pool, J. F.; Drenth, W. *Chem. Phys. Lett.* **1989**, *164*, 581−586.
(5) Orti, E.; Brèdas, J. L.; Clarisse, C. *J. Chem. Phys.* **1990**, *92*, 1228−1235.
(6) Guillon, D.; Skoulios, A.; Piechocki, C.; Simon, J.; Weber, P. *Mol. Cryst. Liq. Cryst.* **1983**, *100*, 275−284.
(7) van der Pol, J. F.; Neeleman, E.; Zwikker, J. W.; Nolte, R. J. M.; Drenth, W.; Aerts, J.; Visser, R.; Picken, S. J. *Liq. Cryst.* **1989**, *6*, 577−592.
(8) Engel, M. K.; Bassoul, P.; Bosio, L.; Lehmann, H.; Hanack, M.; Simon, J. *Liq. Cryst.* **1993**, *15*, 709−722.
(9) Van Nostrum, C. F.; Bosman, A. W.; Gelinck, G. H.; Schouten, P. G.; Warman, J. M.; Ketgens, A. P. M.; Devillers, M. A. C.; Meijerink, A.; Picken, S. J.; Sohling, U.; Schouten, A.-J.; Nolte, R. J. M. *Chem. Eur. J.* **1995**, *1*, 171−182.
(10) Kroon, J. M.; Koehorst, R. B. M.; Van Dijk, M.; Sanders, G. M.; Sudhölter, E. J. R. *J. Mater. Chem.* **1997**, *7*, 615−624.
(11) Clarkson, G. J.; Cook, A.; McKeown, N. R.; Treacher, K. E.; Ali-Adib, Z. *Macromolecules* **1996**, *29*, 913−917.
(12) Hatsusaka, K.; Ohta, K.; Yamamoto, I.; Shirai, H. *J. Mater. Chem.* **2001**, *11*, 423−433.
(13) Schouten, P. G.; Van der Pol, J. F.; Zwikker, J. W.; Drenth, W.; Picken, S. J. *Mol. Cryst. Liq. Cryst.* **1991**, *195*, 291−305.
(14) van Nostrum, C. F.; Bosman, A. W.; Gelinck, G. H.; Picken, S. J.; Schouten, P. G.; Warman, G. M.; Schouten A. J.; Nolte, R. J. M. *J. Chem. Soc. Chem. Commun.* **1993**, 1120−1122. Collard, D. M.; Lillya, C. P. *J. Am. Chem. Soc.* **1989**, *111*, 1829−1830.
(15) Lillya, C. P. *J. Am. Chem. Soc.* **1989**, *111*, 1829−1830.
(16) Schouten, P. G.; Warman, J. M.; de Haas, M. P.; van der Pol, J. F.; Zwikker, J. W. *J. Am. Chem. Soc.* **1992**, *114*, 9028−9034.
(17) Schouten, P. G.; Warman, J. M.; de Haas, M. P.; van Notrum, C. F.; Gelinck, G. H.; Nolet, R. J. M.; Copyn, M. J.; Zwikkler, J. W.; Engel, M. K.; Hanack, M.; Chang, Y. H.; Ford, W. T. *J. Am. Chem. Soc.* **1994**, *116*, 6880−6894.

10.1021/cm050165c CCC: $30.25
Published on Web 05/06/2005

Generally, Pc-based applications require fabrication of deposited films. Therefore, understanding of the columnar arrangement in the Pc films at the scale ranging from the individual columnar diameter to some micrometers is of great interest. However, this range (i.e., the meso-scale) falls in the gap between the range probed by conventional X-ray scattering and that of optical microscopy measurements. Among the techniques that can provide information on these length scales, atomic force microscopy (AFM) is probably the most suitable due to its nondestructive character and applicability to nonconductive samples. In the past, visualization of columnar structure and orientation has mainly been carried out on highly organized thin and ultrathin Pc films prepared by sublimation or by the Langmuir−Blodgett technique.[18−21] Information on thicker and less-ordered Pc films (e.g., prepared by spin-coating or dipping) is practically absent in the literature. This is an unfortunate omission since the latter techniques are suitable for processing on an industrial scale.

Here we report on the structure and thermotropic behavior of four newly synthesized metal-free alkoxy tetrasubstituted Pcs with branched aliphatic chains. Phase characterization was done with classical techniques such as X-ray diffraction on oriented samples, polarized optical microscopy (POM), and differential scanning calorimetry (DSC), as well as, to our knowledge, the first meso-scale characterization of columnar structure in relatively thick films of mesomorphic Pcs performed using tapping mode AFM employing the new generation ultra-sharp tips.[22] Previously we have used these tips to study the columnar structure of a mesomorphic star-shaped molecule.[23]

Experimental Section

Materials. The synthesis of the studied Pcs and purification methods are described elsewhere.[24] The structure of the studied Pc molecules is shown schematically in Figure 1. The branching point has been kept the same for all the derivatives, while the length of the branch and that of the main chain vary.

Methods. An optical microscope (Olympus Provis AX 70) coupled to a Linkam heating stage was used for optical texture observations. The samples were placed between glass slides. The thermal behavior was studied using a Mettler-Toledo heat-flux DSC-822^e at a heating rate of 10 °C/min under helium atmosphere.

Oriented samples of Pcs, in the form of fibers of approximately 0.7-mm diameter, were prepared with a home-built mini-extruder. X-ray diffraction measurements were performed on beamline BM26B of the European Synchrotron Radiation Facility (ESRF, Grenoble) using X-ray photons with an energy of 10 keV.[25] The diffraction patterns were collected in the transmission geometry. The sample temperature was controlled by a Linkam heating stage. The *s*-axis, with $s = 2\sin(\theta)/\lambda$, where θ is the Bragg angle and λ is the wavelength, was calibrated using silver behenate.

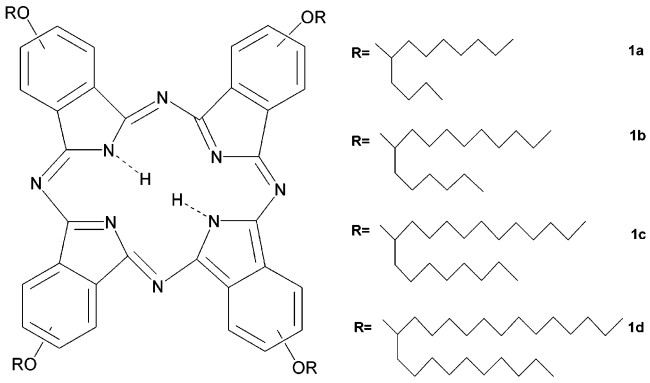

Figure 1. Molecular structure of Pc derivatives **1a**−**d**.

Atomic force microscopy was used to investigate the surface morphology of spin-coated films in tapping mode. The instrument used was a Digital Instruments Nanoscope III. High-resolution images were obtained using standard tapping mode Si tips and Hi'Res probes (Mikromasch) with ultrasharp whiskers.

Data Analysis. Processing of the 2D X-ray patterns was performed using homemade external compiled modules (XOP) for IGOR PRO (Wavemetrics Ltd.).

The quantitative analysis of AFM images was performed in reciprocal space similarly to the classical treatment of small-angle X-ray scattering (SAXS) curves. The two-dimensional power spectral density function ($P_2(\underline{s})$) was computed from AFM images ($u(\underline{r})$) up to the critical, or Nyquist, frequency depending upon the experimental sampling interval as

$$P_2(\underline{s}) \equiv \frac{1}{A}\left|\int_A u(\underline{r})W(\underline{r})\exp(2\pi i\underline{s}\cdot\underline{r})d^2\underline{r}\right|^2 \qquad (1)$$

where A denotes the image area, $W(\underline{r})$ is a window function,[26] and $\underline{s}$ is the 2D reciprocal space vector. The $P_2(\underline{s})$ function was then transformed into the one-dimensional power spectral density function ($P_1(s)$), where s stands for the norm of $\underline{s}$, according to

$$P_1(s) = (2\pi s)^{-1}\int P_2(\underline{s}')\delta(|\underline{s}'| - s)d\underline{s}' \qquad (2)$$

The real part of the Fourier transform of $P_1(s)$ corresponds to the one-dimensional SAXS-type correlation function[27]

$$\gamma(l) \cong Re\{2\pi\int_0^\infty P_1(s)s\exp(2\pi isl)\exp(4\pi^2\sigma^2s^2)ds\} \qquad (3)$$

In eq 3 we have modified the $P_1(s)$ function assuming sigmoidal gradient transition layers having thickness σ[28] instead of a sharp interface. Since the absolute values of the power spectral density function of AFM images do not have any particular physical meaning, the function $\gamma(l)$ was normalized ($\gamma(0) = 1$). The interface distribution function $\gamma''(l)$, defined as the convolution of the first

(18) Vèlez, M.; Vieira, S.; Chambrier, I.; Cook, A. M. *Langmuir* **1998**, *14*, 4227−4231.
(19) Smolenyak, P.; Peterson, R.; Nebesny, K.; Türker, M.; O'Brien, D. F.; Armstrong, N. R. *J. Am. Chem. Soc.* **1999**, *121*, 8628−8636.
(20) Drager, A. S.; Zangmeister, R. A. P.; Armstrong, N. R.; O'Brien, D. F. *J. Am. Chem. Soc.* **2001**, *123*, 3595−3596.
(21) Zangmeister, R. A. P.; O'Brien, D. F.; Amstrong, N. R. *Adv. Funct. Mater.* **2002**, *12*, 179−186.
(22) Klinov, D.; Magonov, S. *Appl. Phys. Lett.* **2004**, *84* (14), 2697−2699.
(23) Gearba, R. I.; Bondar, A.; Lehmann, M.; Goderis, B.; Bras, W.; Koch, M. H. J.; Ivanov, D. A. *Adv. Mater.* **2005**, *17*, 671−676.
(24) Tant, J. Discotic liquid crystals as organic semiconductors for photovoltaic device applications. Ph.D. Thesis, Universitè Libre de Bruxelles, Brussels, Belgium, 2004.
(25) Bras, W.; Dolbnya, I. P.; Detollenaere, D.; van Tol, R.; Malfois, M.; Greaves, G. N.; Ryan, A. J.; Heeley, E. *J. Appl. Crystallogr.* **2003**, *36*, 791−794.
(26) Press, W. H.; et al. *Numerical Recipes in C, The Art of Scientific Computing*; Plenum Press: New York 1988.
(27) Ruland, W. *Colloid. Polym. Sci.* **1977**, *255*, 417−427.
(28) Koberstein, J. T.; Morra, B.; Stein, R. S. *J. Appl. Crystallogr.* **1980**, *13*, 34−45.

Table 1. Thermotropic Behavior of Pc Derivatives 1a−d

compound	phase transition temperature (onset) [°C] /enthalpy change, ΔH [kJ/mol][a]
1a	heating: Col_r 79/[b]Col_h
1b	heating: Col_r 90.7/−0.4 Col_h
	cooling: Col_h 81/0.4 Col_r
1c	heating: Col_r 65/−0.008 Col_h 212/−6.6 I
	cooling: I 225/8.7 Col_h − Col_r (not detectable in DSC)
1d	heating: Col_r 46/−0.006 Col_h 166/−3.2 I
	cooling: I 171/3.6 Col_h 49/0.004 Col_r

[a] Col_r, columnar rectangular mesophase; Col_h, columnar hexagonal mesophase; I, isotropic phase. [b] Transition observed only in POM.

derivatives of the AFM profile across the columnar stack

$$\gamma''(l) = \frac{d\rho(l)}{dl} \times \frac{d\rho(-l)}{dl} \tag{4}$$

was calculated as the second derivative of $\gamma(l)$

$$\gamma''(l) = \frac{d^2\gamma(l)}{dl^2} \tag{5}$$

The function $\gamma''(l)$ was used to calculate morphological parameters of the columnar structure such as the most probable core size (D_{core}) and lateral chain thickness (D_{chains}). This is possible due to the fact that $\gamma''(l)$ can be expanded in a series of different interface distribution functions with alternating signs[29]

$$\gamma''(l) \cong h_{core}(l) + h_{chains}(l) - 2h_{col}(l) + ... \tag{6}$$

The first three distribution functions in eq 6 are used in the present study, i.e., the core thickness distribution, $h_{core}(l)$, the lateral chains thickness distribution, $h_{chains}(l)$, and the distribution of the intercolumnar distance, $h_{col}(l)$. More details of the method can be found in previous publications.[30−31]

Results and Discussion

Optical observations revealed common morphological transitions occurring on cooling Pc derivatives **1a**−**d** (see Table 1). Characteristic textures of molecule **1d** are shown in Figure 2. One can see a classical fan-shaped texture, indicative of a hexagonal columnar mesophase,[13] Col_h, which appears during cooling the material from the isotropic state (Figure 2, top panel). On further cooling, additional morphological features in the form of striations, forming a crosshatch, appear (Figure 2, bottom panel). This can be attributed to a columnar rectangular mesophase Col_r.[13,32] The transition to Col_r is also accompanied by a decrease in the overall birefringence. This made it possible to accurately determine the Col_h−Col_r transition temperature during cooling the material by automatically recording optical images with the help of a digital camera. The integrated image intensity for molecules **1a** and **1d** is given as a function of temperature in Figure 3A. These molecules, as well as two others (not shown here), reveal the described phase transition

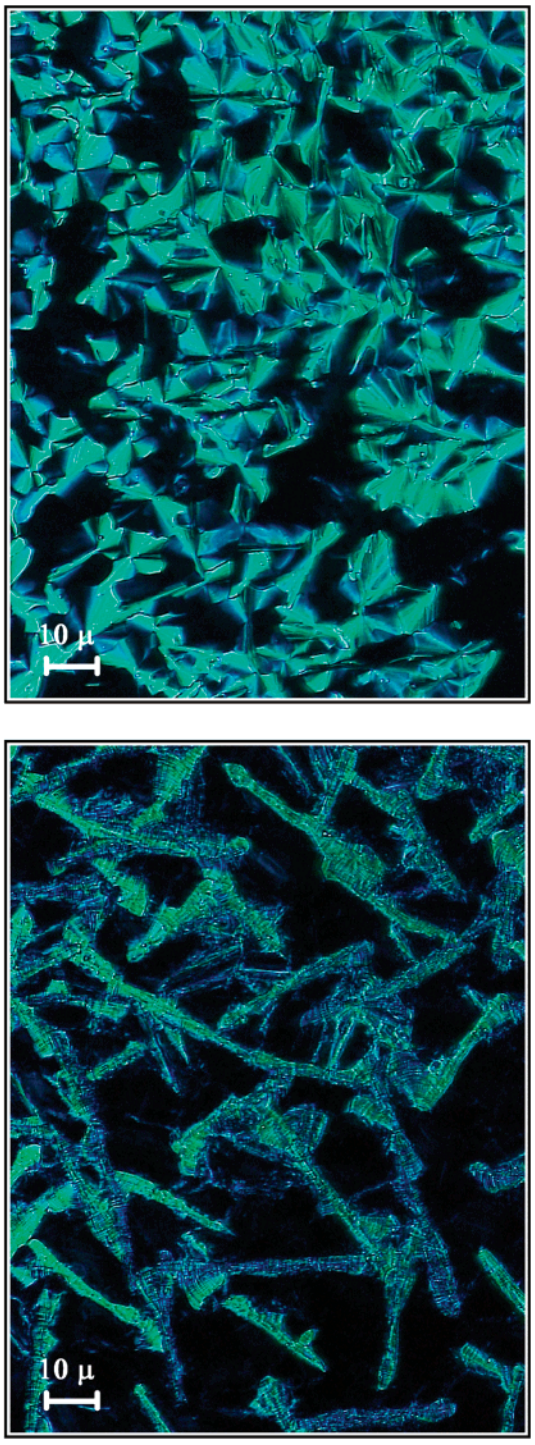

Figure 2. Optical textures of **1d** viewed between crossed polars: columnar hexagonal mesophase at 110 °C (top panel) and columnar rectangular phase at room temperature (bottom panel).

between a rectangular and a hexagonal columnar mesophase. At higher temperatures, a strong decrease of the optical intensity, related to the sample isotropization, is observed for the molecules with longer aliphatic alkyl chains, i.e., **1c** and **1d**. No crystalline phase was detected in the temperature range under investigation, i.e., from RT up to 230 °C.

Table 1 summarizes the data on thermotropic behavior of **1a**−**d**. Note that the isotropization temperature decreases with increasing main alkyl chain length. This trend is paralleled by the Col_r−Col_h transition with the exception of the **1a** derivative. We would like to stress here that the optical

(29) Balta-Calleja, F. J.; Vonk, C. G. *X-ray Scattering of Synthetic Polymers*; Elsevier: Amsterdam, 1989.
(30) Basire, C.; Ivanov, D. A. *Phys. Rev. Lett.* **2000**, *85*, 5587−5590.
(31) Ivanov, D. A.; Magonov, S. Atomic Force Microscopy Studies of Semicrystalline Polymers at Variable Temperature. In *Polymer Crystallization: Observations, Concepts and Interpretations*; Sommer, J. U., Reiter, G., Eds.; Springer-Verlag: Berlin, 2003; pp 98−129.
(32) Mamlok, L.; Malthete, J.; Tinh, N. H.; Destrade, C.; Levelut, A. M. *J. Phys. Lett.* **1982**, *43*, 641−647.

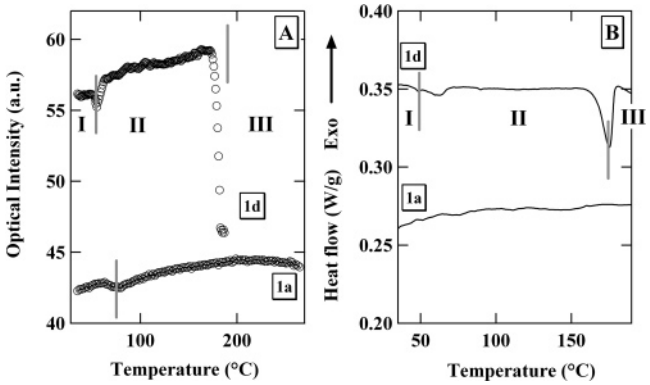

Figure 3. Polarized optical microscopy and differential scanning calorimetry results: (A) Integrated optical intensity for **1a** and **1d** measured at a constant cooling rate of 1 °C/min; (B) DSC heating curves corresponding to the same Pc molecules as in A; the curves have been vertically offset for clarity.

intensity measurements complement standard DSC analysis since the Col_h-Col_r transition of Pcs is not always detectable by DSC.[6] For instance, the thermograms corresponding to molecules **1a** and **1d** (Figure 3A) show that the Col_h-Col_r transition is detectable for the former but not for the latter. Generally, the enthalpy change associated with this mesophase−mesophase transition is rather small for all Pc derivatives used in this work (Table 1).

The supramolecular organization of Pcs **1a**−**d** was studied by performing X-ray diffraction experiments on oriented samples. The results are summarized in Table 2. All the compounds show a columnar rectangular disordered mesophase, Col_{rd}, at RT and a columnar hexagonal ordered mesophase, Col_{ho}, at 110 °C. Fiber diffraction patterns of both phases are shown in Figure 4. The small-angle fiber diffraction patterns in the Col_{ho} mesophase (Figure 4A) show a set of equatorial reflections with *s*-spacings given by the ratio $1:\sqrt{3}:2:\sqrt{7}$. These can be indexed as the 100, 110, 200, and 210 reflections of an oriented hexagonal columnar mesophase. The wide-angle diffraction region of the same pattern displays two diffraction features: A broad halo is found at $s = 0.23$ Å^{-1}. This is believed to arise from the diffraction of the side-chains in the liquidlike state.[33] The direct space distance is approximately 4.5 Å, which is in good agreement with the van der Waals radius of the carbon atom.[34] The second wide-angle peak (denoted P in the figure) can be accounted for by assuming stacking of molecules in columns with an average nearest neighbor distance of 3.4−3.5 Å. The presence of this reflection implies a certain degree of order in the placement of molecules in the column. Therefore the corresponding mesophase was identified as hexagonal ordered columnar mesophase. Note that the distinction between the ordered and disordered columnar phases is more a matter of convention. Despite the fact that the P peak in the low-temperature mesophase is characterized by about the same width at half-maximum (0.027 Å^{-1}) as the corresponding peak of the Col_{ho} phase (0.024 Å^{-1}), it is a common practice to identify the columnar rectangular mesophase as Col_{rd} (disordered).[33,35] Interestingly, some years ago a claim was made that the ordered mesophases cannot exist for nonhexagonal columnar mesophases.[33] The latter statement does not seem to hold for the systems studied in this work, i.e., rectangular mesophases that are only slightly different from hexagonal structures (pseudohexagonal lattices).

In the diffractograms corresponding to the low-temperature mesophase of **1a**−**d** derivatives (cf. Figure 4B and C) six reflections are present in the small-angle region. The crystallographic indexation of these reflections is given in the figures and in Table 2. Since all *hk*0 reflections, denoted further as *hk* with $h + k \neq 2n$, *h*0 with $h \neq 2n$, and 0*k* with $k \neq 2n$, are absent, this is consistent with the sample being in the crystallographic register described by the two-dimensional space group *C*2*mm*.[36] At high scattering angles the diffraction patterns exhibit only a broad peak, reflecting the disordered state of the lateral chains and the P reflection corresponding to the form-factor of the column. The tilt of the molecules with respect to the columnar axis was measured from the angular dispersion of the scattering intensity of the P peak (Figure 4D), which is given as follows:

$$\boldsymbol{I}(\phi) = \int_{s_1}^{s_2} I(s,\phi)ds \qquad (7)$$

In eq 7 s_1 and s_2 denote the limits of the radial integration of the intensity $I(s,\phi)$ represented in polar coordinates. Note that the azimuthal scan (Figure 4D) displays two broad maxima, which indicate a certain distribution of the tilt angles of the disks. The location of the intensity maxima[37] was taken as the most probable disk tilt angle ϕ, which ranges between 15 and 18° (cf. Table 1). If we assume that the sample is described by *C*2*mm* space group, one can conclude that the disks are tilted either along *a* or along *b* directions. Since the smaller of the *a* and *b* lattice parameters (chosen in this work as *b*) is close to the *a* parameter of the corresponding hexagonal mesophase, whereas the other (in this case *a*) is systematically smaller than $\sqrt{3}$ times the hexagonal lattice parameter, one can conclude that the disks are tilted along *a*. The theoretical tilt angle calculated for this symmetry group assuming the planarity of molecules is given as

$$\phi = \arccos\left(\frac{a}{b\sqrt{3}}\right) \qquad (8)$$

The values of the tilt calculated with eq 8 given in Table 2 show a rather good agreement with the experimental values, which supports the choice of the symmetry group. The knowledge of the c parameter (termed $\pi-\pi$ stacking), which corresponds to the position of the maximum of the P peak, and of the disk tilt is required for calculation of the mesophase density (cf. Table 2).

(33) Levelut, A. M. *J. Chim. Phys.* **1983**, *80*, 149−161.
(34) Bondi, A. *J. Phys. Chem.* **1964**, *68*, 441−451.
(35) Destarde, C.; Foucher, P.; Gasparoux, H.; Tinh, N. H.; Levelut, A. M.; Malthete, J. *Mol. Cryst. Liq. Cryst.* **1984**, *106*, 121−146.
(36) *International Tables for Crystallography*, 1st ed.; Kluwer Academic Publishers: Boston, MA, 2002; Vol. A, p 100.
(37) It should be mentioned that, in some instances, the azimuthal distributions of the P peak were found to be slightly different for the lower and upper parts of the 2D diffraction patterns: the peaks in the upper part appear to be better resolved. This could be accounted for by a small misalignment of the image plate. Therefore, the analysis was performed only for the upper parts of the patterns.

Table 2. Temperature-Dependent X-ray Diffraction Data on Oriented Samples 1a−d

mesophase	hk	d_{exp} [Å]	d_{calc} [Å]	lattice parameters a and b [Å]	ϕ exp. [deg]	ϕ^a theor. [deg]	$V(CH_2)^b$ [Å^3]	density^c [g/cm^3]
				Pc84 (**1a**)				
Col_{rd}	11	22.3	22.3	$a = 42.0$	18	22	29.6	1.07
(RT)	20	21.0	21.0	$b = 26.3$				
	02	13.1	13.1					
	31	12.3	12.3					
		4.8 (halo)						
		3.4 ($\pi-\pi$ stacking)						
Col_{ho}	10	23.0	23.0	$a = 26.5$			28.4	1.04
(110 °C)	11	13.2	13.3					
	20	11.5	11.5					
	21	8.6	8.7					
		4.8 (halo)						
		3.4 ($\pi-\pi$ stacking)						
				Pc106 (**1b**)				
Col_{rd}	11	24.0	24.1	$a = 45.0$	15	24	24.2	1.09
(RT)	20	22.5	22.5	$b = 28.5$				
	02	14.2	14.2					
	31	13.2	13.3					
	22	12.1	12.0					
	40	11.3	11.3					
		4.7 (halo)						
		3.4 ($\pi-\pi$ stacking)						
Col_{ho}	10	24.5	24.5	$a = 28.2$			25.9	1.07
(110 °C)	11	14.1	14.1					
	20	12.2	12.2					
	21	9.2	9.2					
		5.0 (halo)						
		3.4 ($\pi-\pi$ stacking)						
				Pc128 (**1c**)				
Col_{rd}	11	25.9	25.9	$a = 48.6$	15	23	23.8	1.09
(RT)	20	24.4	24.3	$b = 30.6$				
	02	15.3	15.3					
	31	14.2	14.3					
	22	13.1	13.0					
	40	12.1	12.2					
		4.7 (halo)						
		3.4 ($\pi-\pi$ stacking)						
Col_{ho}	10	26.4	26.3	$a = 30.4$			26.5	1.00
(110°C)	11	15.2	15.2					
	20	13.1	13.2					
	21	9.9	10.0					
		4.8 (halo)						
		3.5 ($\pi-\pi$ stacking)						
				Pc1410 (**1d**)				
Col_{rd}	11	27.5	27.4	$a = 52.5$	15	19	23.7	1.07
(RT)	20	26.4	26.3	$b = 32.1$				
	02	16.0	16.1					
	31	15.2	15.4					
	22	13.7	13.7					
	40	13.0	13.1					
		4.6 (halo)						
		3.4 ($\pi-\pi$ stacking)						
Col_{ho}	10	27.6	27.6	$a = 31.8$			24.7	1.04
(110 °C)	11	15.9	15.9					
	20	13.7	13.8					
	21	10.4	10.4					
		4.8 (halo)						
		3.5 ($\pi-\pi$ stacking)						

[a] The tilt angle calculated with the help of eq 8. [b] $V(CH_2)$ = volume of the CH_2 group (see text for more details). [c] Density, ρ, was calculated as $\rho = M_w \cdot Z/(N_A \cdot V_{unit\ cell})$, where $V_{unit\ cell}(Col_{hd}) = a^2 \cdot c \cdot \sqrt{3}/2$ and $V_{unit\ cell}(Col_{rd}) = a \cdot b \cdot c$, M_w is the molecular weight, and $Z = 1, 2$ for the hexagonal and centered rectangular mesophase, respectively.

From Figure 5 and Table 2 one can conclude that the lattice parameter of the Col_{ho} phase increases with the main chain length, from 26.5 Å for molecule **1a** which has short lateral chains, to 31.8 Å for the **1d** molecule, which has long lateral chains. By approximating the variation of *a*, as a function of the number of carbons (*n*) in the main chain, by a straight line and by extrapolating the fit to the intersection with the *y*-axis (Figure 5), one can estimate the diameter of the molecular core including the bridging ether oxygens. This value (19.2 Å) is found to be comparable to the literature diameter of 16 Å.[38] Taking the smallest of these values (i.e., 16 Å) and assuming the alkyl chains to adopt the all-*trans* conformation, the calculated molecular diameter of the studied Pcs was found to vary between 40.0 and 55.2 Å.

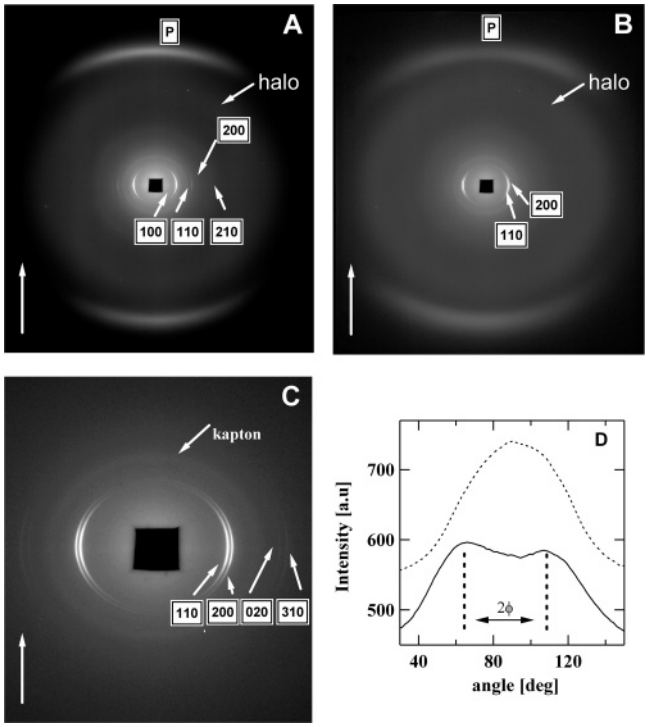

Figure 4. 2D X-ray diffraction data on oriented samples, the white arrows in A−C indicate the fiber axis orientation: (A) diffraction pattern of **1a** recorded at 110 °C; (B) the same as in A recorded at room temperature, with a zoom of the low s-range given in (C). The diffuse reflection in the small-angle region indicated by the oblique arrow in (C) corresponds to the Kapton tape used to fix the sample; (D) angular dispersion of the P reflection for the rectangular and hexagonal (dotted line) mesophases of **1a** (the curves are vertically offset for clarity). The integration in D was performed between the s-values of 0.28 and 0.33 $Å^{-1}$.

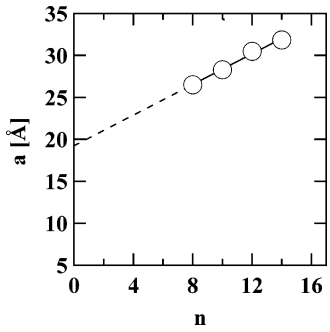

Figure 5. Variation of the lattice parameter of the hexagonal columnar mesophase at 110 °C with the number of carbon atoms in the main chain. Extrapolation of the linear fit to the data (dashed and solid lines) allows estimation of the diameter of the rigid core.

These values are significantly larger than the ones derived from the X-ray measurements. A possible explanation of this discrepancy is the interdigitation of the lateral chains belonging to the molecules in the neighboring columns. More insight into the lateral chain conformation can be obtained from the estimate of the molecular volume. On one hand, by using the lattice parameters determined from the X-ray measurements, the volume of one molecule in the hexagonal and rectangular mesophases can be written as $a^2 \cdot c \cdot \sqrt{3}/2$ and $a \cdot b \cdot c/2$, respectively. On the other hand, the molecular volume V_c can be expressed as $V_c = V_0 + ZnV_{CH2}$, where V_0 is the volume of the molecular core without the methylene groups and Z is the number of lateral chains. Equating both volumes, one can find that the V_{CH2} value varies between 24.7 and 28.4 $Å^3$ (cf. Table 2). Similar estimates are also found for the low-temperature rectangular mesophase Col_{rd}. These values are in some instances smaller than the literature values for the columnar mesophases (27−28 $Å^3$);[39] this discrepancy can be explained by the fact that the V_{CH2} can differ for linear and branched alkyl chains.

The structure and columnar orientation in thick spin-coated films was studied by AFM. Figure 6A shows the large-scale morphology of an approximately 100-nm thick film of **1d** visualized shortly after the spin-coating. The film shows a multilayer structure, the individual layer thickness in which can be determined using the corresponding height histogram shown in the insert. The height difference between the two maxima of the histogram is approximately 3.1 nm, which is close to the distance between the 110 planes found from the X-ray diffraction experiments (cf. Table 2). A small-scale tapping mode amplitude image (Figure 6B) taken with an ultrasharp tip reveals the details of the columnar structure of the film. It is visible that the columns are oriented with their columnar axes in the plane of the substrate. This supports the assignment of the layer thickness to the distance of the 110 X-ray peak.

The image in Figure 6B was recorded in a region with steplike defects due to the occurrence of incomplete layers. This is similar to the ones present in Figure 6A. The layer boundaries (indicated by arrows in the figure) appear in the image as thick black stripes. A detailed analysis of the columnar orientation near these boundaries indicates that in some instances the columns are running parallel or at some angle with respect to the steps (cf. arrows 1 and 2), without any distortion of the structure at the boundary. In this case it is clear that the columns belonging to successive layers are locally in register. In other instances, the step defects delimit LC domains with different columnar orientations (cf. arrow 3). However, even then the domain boundaries do not always disrupt the columnar structure, i.e., the columns pass from one domain to the other without breaking by adopting a certain curvature in the proximity of the boundary. Some other examples of regions with curved columns can be seen in the small-scale phase images given in Figure 6C and D. Thus, the image in Figure 6C shows a single LC domain with slightly curved columns, where the columnar curvature spans over the entire image and is not visibly related to the presence of a domain boundary. By contrast, Figure 6D shows a situation similar to the one observed in Figure 6B where the columnar curvature is clearly induced by the layer boundaries. The columns pass across one of the boundaries (arrow 1) without breaking, whereas the other boundary (arrow 2) completely disrupts the columnar structure making columns in neighboring regions uncorrelated.

The AFM phase contrast observed in Figure 6C and D is supposed to be due to a difference in the local material properties pertinent to the molecular core (rigid part) and the lateral alkyl chains (soft part). The visualization by AFM

(38) Weber, P.; Guillon, D.; Skoulios, A. *Liq. Cryst.* **1991**, *9* (3), 369−382.

(39) Levelut, A. M.; Malthete, J.; Destrade, C.; Tinh, N. H. *Liq. Cryst.* **1987**, *2* (6), 877−888.

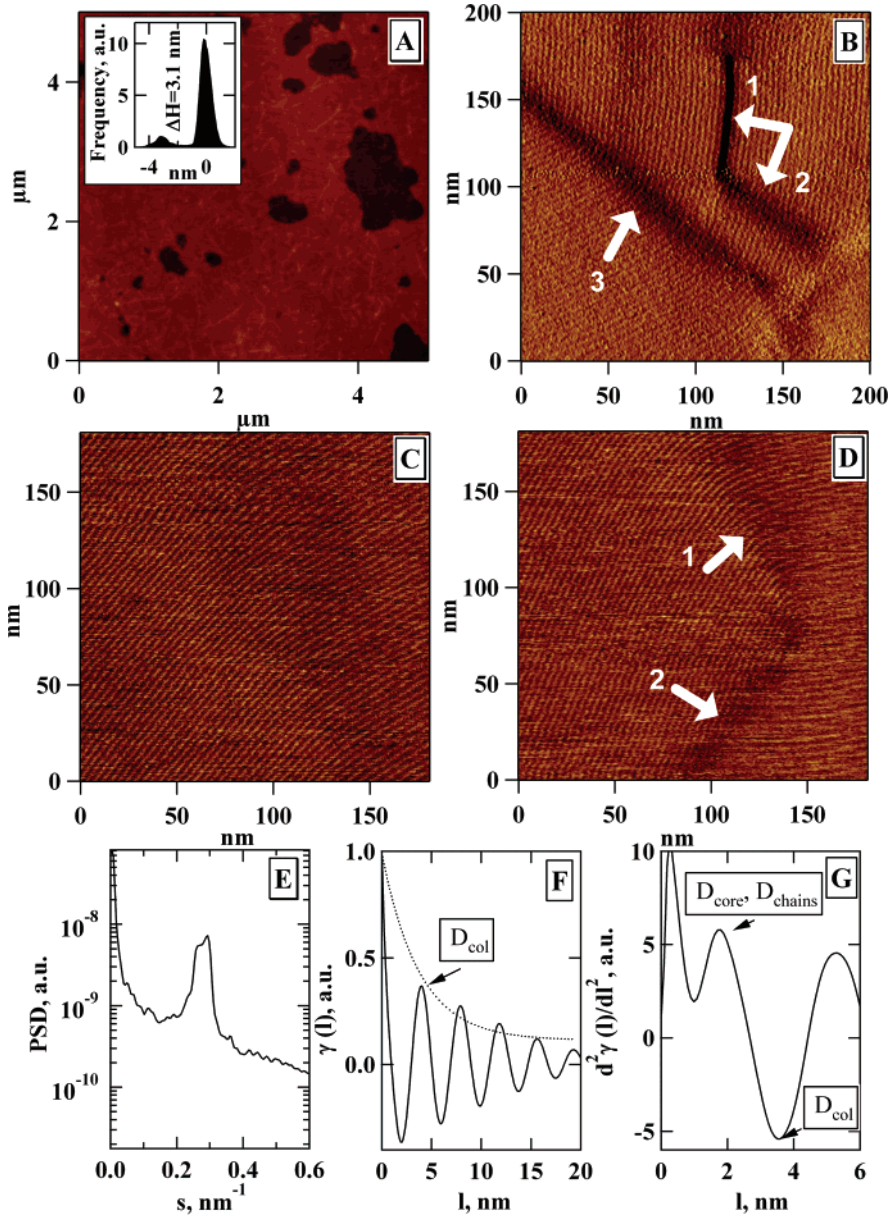

Figure 6. Tapping mode AFM images of a mesomorphic spin-coated film of **1d**. (A) Large-scale topography image showing a layerlike structure of the film, the height histogram given in the inset reveals the layer thickness of 3.1 nm. (B−D) Small-scale tapping amplitude (B) and phase (C and D) images of the columnar structure. The arrows in (B) and (D) point at the layer and domain boundaries, which can be parallel or oblique to the column direction (see the text for more details). (E) One-dimensional power spectral density function corresponding to the image in (C). (F and G) One-dimensional SAXS-type correlation function and interface distribution function, respectively. Dotted line in (F) shows a fit of the subsidiary maxima of the correlation function with an exponential function to find the correlation length of the structure.

of the columnar structure and the possibility to discriminate between different parts of the structure in the phase inspired us to perform quantitative reciprocal space analysis of AFM images. This has been developed previously for the characterization of semicrystalline polymer structures.[30] A typical one-dimensional power spectral density function (PSD) given in Figure 6E exhibits a well-pronounced peak located at about 0.29 nm^{-1}, which can be attributed to the regular spacing between the columnar axes. The corresponding one-dimensional SAXS-type correlation and interface distribution functions are given in Figure 6F and G, respectively. The periodicity of the structure determined from the first subsidiary maximum of the correlation function is 3.6 nm. This is in reasonable agreement with the intercolumnar distance, D_{col}, in the 110 plane of the Col_{rd} phase of **1d** (3.1 nm) determined by X-ray diffraction. Therefore, the conclusions on the 110 film surface orientation are supported by both the vertical and lateral AFM measurements. A more refined analysis of the structure was carried out with the help of the interface distribution function (Figure 6G), from which the thickness of regions occupied by the molecular core and by the lateral chains can be determined. In our case, the positive subsidiary peaks denoted D_{core} and D_{chains} merge in one single peak indicating that the two distances are close to each other, i.e., equal to one-half of the columnar diameter. The latter estimation is in good agreement with the value obtained by extrapolating the columnar diameter to the zero length of the lateral chain (Figure 5).

The degree of order in the studied films was characterized by the height decrease of the subsidiary maxima of the

correlation function, which was fitted to a simple exponential function (dotted line in Figure 6F). The correlation length resulting from this fit (3.7 nm) is quite small and comparable to a single intercolumnar distance. Importantly, the application of Scherrer's equation to the X-ray fiber diffraction data results in the correlation length of 8.3 nm, i.e., somewhat higher than the value determined by AFM. This difference can be explained by assuming an increased column ordering in the extruded fibers compared to the spin-coated films, which exhibit various structural defects such as the columnar curvature.

Acknowledgment. This work was supported by the Communauté Française de Belgique (ARC 00/05-257). We are grateful to J. Tant and Y. Geerts (Université Libre de Bruxelles, Belgium) for providing the Pc molecules, and F. Meneau (BM26B, ESRF) for the assistance in the X-ray measurements. B.G. is a postdoctoral fellow of the Fund for Scientific Research-Flanders (Belgium), FWO-Vlaanderen. We thank FWO-Vlaanderen and Prof. H. Reynaers for their continuous support and D. Detollenaere (FWO-Vlaanderen) and J. Jacobs (NWO) for technical assistance.

CM050165C